

Article

Comparative Catalytic Performance Study of 12-Tungstophosphoric Heteropoly Acid Supported on Mesoporous Supports for Biodiesel Production from Unrefined Green Seed Canola Oil

Fahimeh Esmi, Shima Masoumi  and Ajay K. Dalai *

Catalysis and Chemical Reaction Engineering Laboratories, Department of Chemical and Biological Engineering, College of Engineering, University of Saskatchewan, Saskatoon, SK S7N 5A9, Canada; fae380@mail.usask.ca (F.E.); shm677@mail.usask.ca (S.M.)

* Correspondence: ajay.dalai@usask.ca

Abstract: In this study, three solid acid catalysts, namely mesoporous aluminophosphate-supported 12-tungstophosphoric heteropoly acid (HPW/MAP), mesoporous aluminosilicate-supported 12-tungstophosphoric heteropoly acid (HPW/MAS), and gamma alumina-supported 12-tungstophosphoric heteropoly acid (HPW/ γ -Al₂O₃) were prepared and characterized. Mesoporous aluminophosphate (MAP) and mesoporous aluminosilicate (MAS) were synthesized via sol-gel and hydrothermal methods, respectively, and 25 wt.% of 12-tungstophosphoric heteropoly acid (HPW) was immobilized on the support materials using the wet impregnation method. The features of the fabricated catalysts were comprehensively investigated using various techniques such as BET, XRD, NH₃-TPD, TGA, and TEM. The surface area of the supported catalysts decreased after HPW impregnation according to BET results, which indicates that HPW loaded on the supports and inside of their pores successfully. The density and strengths of the acid sites of the support materials and the catalysts before reaction and after regeneration were determined by the NH₃-TPD technique. Accordingly, an increase in acidity was observed after HPW immobilization on all the support materials. The catalytic performance of the catalysts was studied through alcoholysis reaction using unrefined green seed canola oil as the feedstock. The maximum biodiesel yield of 82.3% was obtained using 3 wt.% of HPW/MAS, with a methanol to oil molar ratio of 20:1, at 200 °C and 4 MPa over 7 h. The reusability study of HPW/MAS showed that it can maintain 80% of its initial activity after five runs.

Keywords: biodiesel; solid acid catalyst; heteropoly acid; reusability; unrefined canola oil



Citation: Esmi, F.; Masoumi, S.; Dalai, A.K. Comparative Catalytic Performance Study of 12-Tungstophosphoric Heteropoly Acid Supported on Mesoporous Supports for Biodiesel Production from Unrefined Green Seed Canola Oil. *Catalysts* **2022**, *12*, 658. <https://doi.org/10.3390/catal12060658>

Academic Editors: Diego Luna and Maria Raspolli Galletti

Received: 26 March 2022

Accepted: 12 June 2022

Published: 15 June 2022

Publisher's Note: MDPI stays neutral with regard to jurisdictional claims in published maps and institutional affiliations.



Copyright: © 2022 by the authors. Licensee MDPI, Basel, Switzerland. This article is an open access article distributed under the terms and conditions of the Creative Commons Attribution (CC BY) license (<https://creativecommons.org/licenses/by/4.0/>).

1. Introduction

The significance of developing alternative renewable energy sources to fossil fuels is undeniable, considering the incremental increase in energy demand, the limited sources of crude oil, and the detrimental impacts of their usage on the environment [1–3]. Many scientists have focused on biodiesel production as a renewable and environmentally friendly energy, which can be achieved through the three different techniques of pyrolysis [4], micro-emulsion [5], and alcoholysis [6].

The most prevalent technique employed for biodiesel synthesis is the alcoholysis process. In this method, fatty acid alkyl ester (FAAE) is achieved from the interaction between plant oils or animal fats with alcohol [7].

The selection of feedstock has a big impact on the total cost of biodiesel production as an essential factor of global commercialization. Due to the population growth, using non-edible oil which is highly available and low cost is a priority. However, the major problem with non-edible oils is that they are rich in free fatty acids (FFAs), which is a challenge for conversion to FAAE [8,9].

A catalyst is also considered an essential factor in biodiesel production, which can be categorized into acid and alkaline catalysts. Currently, the most used commercial catalyst for biodiesel synthesis is the homogeneously base-catalyzed transesterification reaction of plant oils. However, a problem arose from the high amount of FFA that can lead to the creation of undesired reactions, such as saponification reaction in the case of using alkaline catalysts. The formation of soap makes the separation process difficult and costly, and adversely affects the yield of biodiesel production [10,11]. Homogeneous acid catalysts are highly active; however, the generation of effluent stream, solubility in the reaction mixture, and corrosive and toxic features have restricted their application. In contrast, heterogeneous acid catalysts are eco-friendly and their phase difference with reaction media has eased their separation, and they can be reused in a new reaction, which can be highly effective in decreasing the cost of production [10,11].

A wide range of solid acid catalysts have been explored for biodiesel synthesis such as zeolites and zeotypes [12], sulfated metal oxides [13], sulphonic acid group catalysts [14], heteropoly acids (HPAs) and supported HPAs [15,16], and acidic montmorillonite catalysts [17]. In heterogeneously catalyzed reactions, the interaction of the active phase with the support is vital to maintain the catalyst activity during the process and to enhance its reusability [18]. Although solid acid catalysts are favorable for biodiesel synthesis from raw materials with low quality, leaching of acid sites remains the major obstacle of solid acid catalysts [19,20]. Thereby, designing efficient and sustainable solid acid catalysts is still a challenge. The preferable solid acid catalyst for the alcoholysis process should possess high acidity and appropriate structural features to prevent active sites from leaching and minimize diffusion limitations. Among various solid acid catalysts, supported HPAs have presented outstanding catalytic features in acid-catalyzed reactions due to their nontoxicity, special structure, and high Bronsted acidity [21–23]. HPW is the most widely used Kegging-type HPA with higher thermal stability and Bronsted acidity, which has indicated superb catalytic performance in acid-catalyzed reactions [24,25].

Various support materials have been employed for the immobilization of heteropoly acids for different applications. Srilatha et al. [26] studied the esterification reaction of palmitic acid using TPA supported on ZrO_2 catalysts. This resulted in ~95% conversion of palmitic acid to biodiesel with better reusability, confirming the strong interaction between TPA and ZrO_2 . Kumbar et al. [27] reported the use of TiO_2 supported TPA as a suitable solid acid catalyst in the alkylation process. It is reported that titanium oxide improved the catalytic activity, which attributed to the strong attachment between TiO_2 and the active phase. $H_4SiW_{12}O_{40}-SiO_2$, synthesized by a one-step method, was used for biodiesel production [28]. $H_4SiW_{12}O_{40}$ was successfully loaded inside the mesoporous channels of $-SiO_2$, which enhanced reusability and diffusion of the reactants.

In this study, two novel methods were used to fabricate HPW/MAP and HPW/MAS for biodiesel production from unrefined green seed canola oil. To our knowledge, no study has explored the potential of MAP as a support material for immobilized HPW and for its application in biodiesel production. In addition, a novel and simple hydrothermal method was used for the synthesis of MAS, which has not been investigated before.

Comprehensive characterization of the synthesized catalysts was investigated and compared with HPW/ $\gamma-Al_2O_3$. The biodiesel synthesis was studied using synthesized catalysts, and the biodiesel product was characterized for the presence of ester functional groups and its suitability as an engine fuel. The other objective of this study was to explore the reusability of the synthesized catalyst, considered as the main factor for biodiesel production commercialization.

2. Experimental Section

2.1. Materials

Sodium aluminate and phosphoric acid (85% mass) were acquired from Fischer Scientific, Waltham, MA, USA. Tetraethylorthosilicate (TEOS, 25 wt.% in H_2O), tetrapropyl ammonium hydroxide (TPAOH, 1M in water), tetramethyl ammonium hydroxide (TMAOH,

25 wt.% in H₂O), and standards of oleic acid, mono-oleate, di-oleate, tri-oleate, and methyl oleate were all supplied by Sigma-Aldrich, Burlington, MA, USA. Methanol (99%) and ethanol (99%) were provided by Innova Chemical, VWR, Edmonton, AB, Canada. Cetyltrimethylammonium bromide (CTAB) was obtained from Merck, Darmstadt, Germany. Ammonium nitrate (>95%), aluminum hydroxide (>76.5%), 12-tungstophosphoric heteropoly acid (HPW) and γ -Al₂O₃ were provided by Alfa-Aesar, Tewksbury, MA, USA. HPLC grades of acetonitrile (ACN), isopropanol, methanol (MeOH), and hexane were purchased from Fischer Scientific, Waltham, MA, USA. Citric acid was supplied by EMD Chemicals Inc., Darmstadt, Germany. Unrefined green seed canola oil was supplied by Milligan Bio-Tech Inc., Saskatoon, SK, Canada.

2.2. Synthesis of Mesoporous Aluminosilicate (MAS)

For MAS preparation, a solution of 0.4 g sodium aluminate in 55 mL of water was prepared under stirring at ambient temperature. After it had dissolved completely, 24 mL of TEOS and 9 mL of TPAOH were added dropwise to the solution, respectively. An ethanol solution containing 5.5 g of citric acid was then added to the mixture and agitated for 1 h. Later, the mixture was poured into a Teflon bottle to be processed in an oven at 100 °C for two days. The calcination of the obtained material was carried out at 550 °C for 5 h. The solid was then ion-exchanged using ammonium nitrate 1 M. In the final step, the resulting sample was calcined at 500 °C for 5 h.

2.3. Synthesis of Mesoporous Aluminophosphate (MAP)

MAP was fabricated via the sol-gel method. A solution of 11.5 g of CTAB (25% mass) in 100 g water was prepared. A total of 3.5 g of dried aluminum hydroxide precursor was added to the phosphoric acid solution and stirred vigorously for 30 min. The acquired mixture was then mixed with CTAB solution and maintained for 30 min. TMAOH was poured into the prepared mixture slowly until pH 9.5 was achieved and then kept for 72 h before proceeding. The final step of the process is filtration and washing of the obtained material with water followed by drying and calcination at 500 °C for 6 h.

2.4. Impregnation of 12-Tungstophosphoric Heteropoly Acid (HPW) on Supports

HPW/MAS and HPW/MAP were synthesized by the immobilization of 25 wt.% HPW on MAS and MAP through the wet impregnation method. With regards to this, HPW was mixed with methanol to dissolve it completely and then support material was transferred slowly to the solution under stirring and aged for 3 h. In terms of HPW/ γ -Al₂O₃, 25% HPW solution was added dropwise on γ -Al₂O₃ beads until they were completely coated in the solution. The obtained sample was dried at room temperature, accompanied with calcination at 450 °C for 5 h.

2.5. Catalytic Reaction

Biodiesel was synthesized through simultaneous esterification and transesterification reactions in a 100 mL Parr reactor to assess the performance of the catalysts. A total of 35 g of oil was warmed up at 50 °C and then added to methanol (20:1 methanol to oil molar ratio) and 3 wt.% of the catalyst (based on oil weight). The reaction was conducted at preliminary conditions of 200 °C, 4 MPa, and 600 rpm to screen the activity of the catalysts for 7 h. An HPLC characterization technique (Agilent technologies 1200 series, Santa Clara, CA, USA), equipped with two columns of Nova-Pak C18 (4.6 mm × 150 mm) and SpherisoRB5 ODS(2) (4.6 mm × 250 mm) connected in series, was used to analyze the ester phase of the product. Reverse HPLC method was used with two mobile phases containing 50% ACN + 25% isopropanol + 25% MeOH for the solvent A and 50% ACN + 50% (5 isopropanol/4 hexane volume ratio) for the solvent B, based on the timeline shown in Table 1, at 1 mL/min for 28 min. The analysis was performed with a sample injection volume of 10 μ L at the column and a detector temperature of 35 °C and 50 °C, respectively. The peaks were detected using an ELSD detector (Agilent 1260 Infinity II, Santa Clara, CA, USA). HPLC calibration was

conducted using standard chemicals of mono-oleate, di-oleate, tri-oleate, methyl oleate, and oleic acid. Equation (1) was used for the ester yield calculation based on wt.%.

$$\text{Ester yield (\%)} = (\text{weight of methyl ester} / \text{weight of oil phase}) \times 100 \quad (1)$$

Table 1. Timeline of mobile phase usage in HPLC.

Time (min)	A (%)	B (%)
0	100	0
7	100	0
15	0	100
28	0	100

2.6. Catalyst Characterization Techniques

The Brunauer–Emmett–Teller (BET) characterization technique (Micromeritics ASAP 2000, Norcross, GA, USA) was used to determine the surface area, and the pore volume and pore diameter of the catalysts (around 0.2 g of each catalyst was used), using the Barrett–Joyner–Halenda (BJH) method. The metal concentration in the HPW supported catalysts was achieved using an iCAP 7000 Series inductively coupled plasma optical emission spectrometry (ICP-OES) instrument (Thermo Scientific, Waltham, MA, USA). A Fourier transform infrared spectrometer (FTIR, Vertex 60 Bruker, Karlsruhe, Germany) was used for FTIR spectroscopy of pyridine adsorption in the 1700–1400 cm^{-1} region. HPW supported catalysts (around 100 mg) were first immersed in pyridine for 6 h. Then, the samples were heated at 100 °C for 2 h and the pyridine chemisorbed catalysts were analyzed to determine the types of acidic sites (Bronsted and Lewis) of the prepared catalysts. Thermogravimetric analysis (TGA) using a TGA Q-500 analyzer (New Castle, DE, USA) was carried out to obtain the thermal stability of the catalysts. An Advanced Bruker D8 diffractometer (Billerica, MA, USA) with Cu K α radiation was employed to obtain wide-angle X-ray diffraction (XRD) patterns in the scanning range of 10° to 90°. Temperature-programmed desorption of ammonia (NH₃-TPD) equipped with a TCD detector (Micromeritics Instrument Corporation, Norcross, GA, USA) was employed to measure the acidity of the catalysts. For the TPD experiment, the sample (0.04 g) was first pretreated in helium at 300 °C for half an hour. The temperature was then decreased to room temperature in flowing helium (20 mL/min). The catalyst sample was then saturated with 15% NH₃ in helium at a flow rate of 20 mL/min. Then, the sample temperature was increased at a ramp rate of 10 °C/min, with a constant helium flow rate of 20 mL/min, and the spectrum for the desorption of NH₃ was recorded with the TCD with a temperature rise from 100 °C to 600 °C, for the evaluation of the NH₃ desorbed and the total acidity. A transition electron microscopy (TEM) characterization technique (Hitachi HT7700, Tokyo, Japan) with an accelerating voltage of 80 kV was used.

3. Results and Discussion

3.1. Catalyst Characterization

The textural features of the support materials and the HPW supported catalysts obtained from BET analysis and the concentration of tungsten (W) in the HPW supported catalysts obtained from the ICP-OES technique are represented in Table 2. The surface area and pore size of MAS is 703 m^2/g and 5.0 nm, respectively, which are higher than MAP, with the surface area of 581 m^2/g and a pore size of 4.7 nm. The specific surface area of MAS is also higher than $\gamma\text{-Al}_2\text{O}_3$ (297 m^2/g). Impregnation of HPW on the support materials led to a decrease in surface area and pore volume for all of them. This could be attributed to both settling of HPW into the pores and calcination of the HPW supported catalysts at 450 °C for 5 h. In a research study conducted by Pires et al. [29], similar results are observed for the impregnation of HPW on MCM-41, MCM-48, and SBA-15. The larger

average pore size of HPW/MAP compared to that of MAP could be due to the occupation or blocking of the micropores of the support, which led to an increase in the average pore size of HPW/MAP. A similar finding is reported for TPA anchored to two mesoporous aluminosilicates (MAS-7, MAS-9) [30].

Table 2. Textural features and metal concentration of catalysts.

Catalyst	BET Surface Area (m ² /g)	Total Pore Volume (cm ³ /g)	Average Pore Size (nm)	ICP-OES W (wt.%)
γ -Al ₂ O ₃	297	0.82	7.5	-
HPW/ γ -Al ₂ O ₃	195	0.50	7.2	23.2
MAP	581	0.14	4.7	-
HPW/MAP	111	0.08	5.1	22.5
MAS	703 ± 9	0.99 ± 0.03	5.0 ± 0.7	-
HPW/MAS	504	0.68	4.4	22.8

Figure 1 illustrates N₂ adsorption–desorption isotherms for all the support materials and HPW supported catalysts. All the samples indicate IV type isotherms, based on IUPAC classification that shows the mesoporous structure of these catalysts [31]. According to Figure 1a, γ -Al₂O₃ and HPW/ γ -Al₂O₃ exhibit a narrow hysteresis loop of type H1, with closure at about $p/p_0 = 0.6$. Regarding MAP (Figure 1b), a small H1 hysteresis loop closure at about $p/p_0 = 0.9$ is observed, which can be associated with the existence of a narrow range of pores with unconnected structure. MAS and HPW/MAS exhibit an H1 hysteresis loop with closure at about $p/p_0 = 0.45$ [32]. After impregnation of HPW on all three supports, the general shape of HPW supported catalyst isotherms were considerably alike, with the related supports and hysteresis loops remaining in the same region of relative pressure. This shows that the loading of HPW on the support materials does not affect their mesoporous structure. However, the reduction in the amount of adsorption after the impregnation of HPW on the supports suggests that HPW supported catalysts have less surface area compared to support materials because of the occupying of pores with HPW. The BET data confirm the suitability of these support materials due to their high surface area and appropriate porosity for HPW immobilization, which are important physical properties for enhancing catalytic activity.

Pore size distribution curves (Figure 2) were derived using the BJH technique based on adsorption volume data. γ -Al₂O₃ and HPW/ γ -Al₂O₃ curves (Figure 2a) indicate the narrow and uniform pore sizes, with an average of 7 nm. Figure 2b,c present uniform mesopores in the average distribution range of 2.5–6.5 nm for MAP and HPW/MAP, and 2–6 nm for MAS and HPW/MAS.

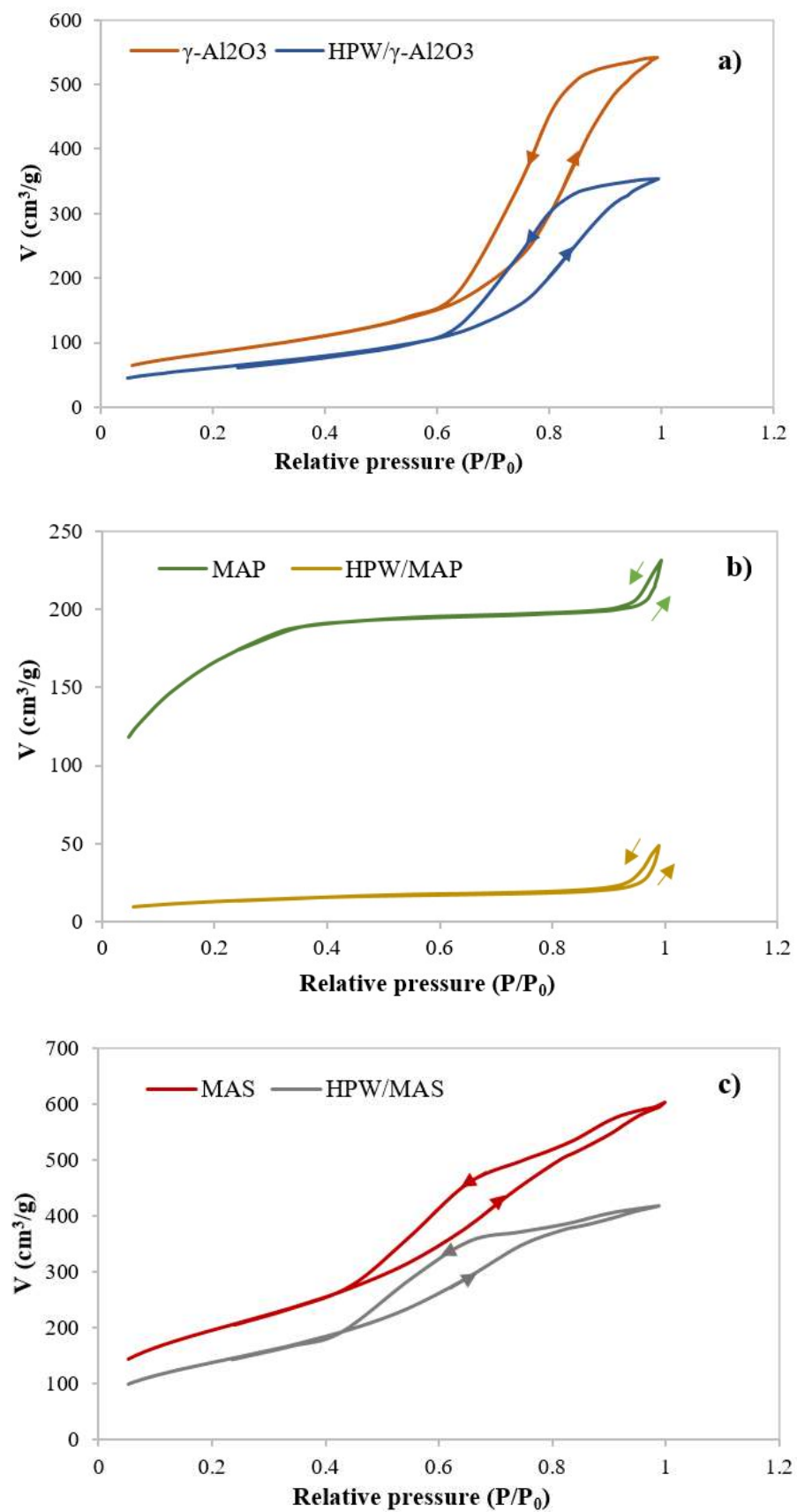


Figure 1. N_2 adsorption–desorption isotherms for (a) $\gamma-Al_2O_3$ and HPW/ $\gamma-Al_2O_3$, (b) MAP and HPW/MAP, and (c) MAS and HPW/MAS.

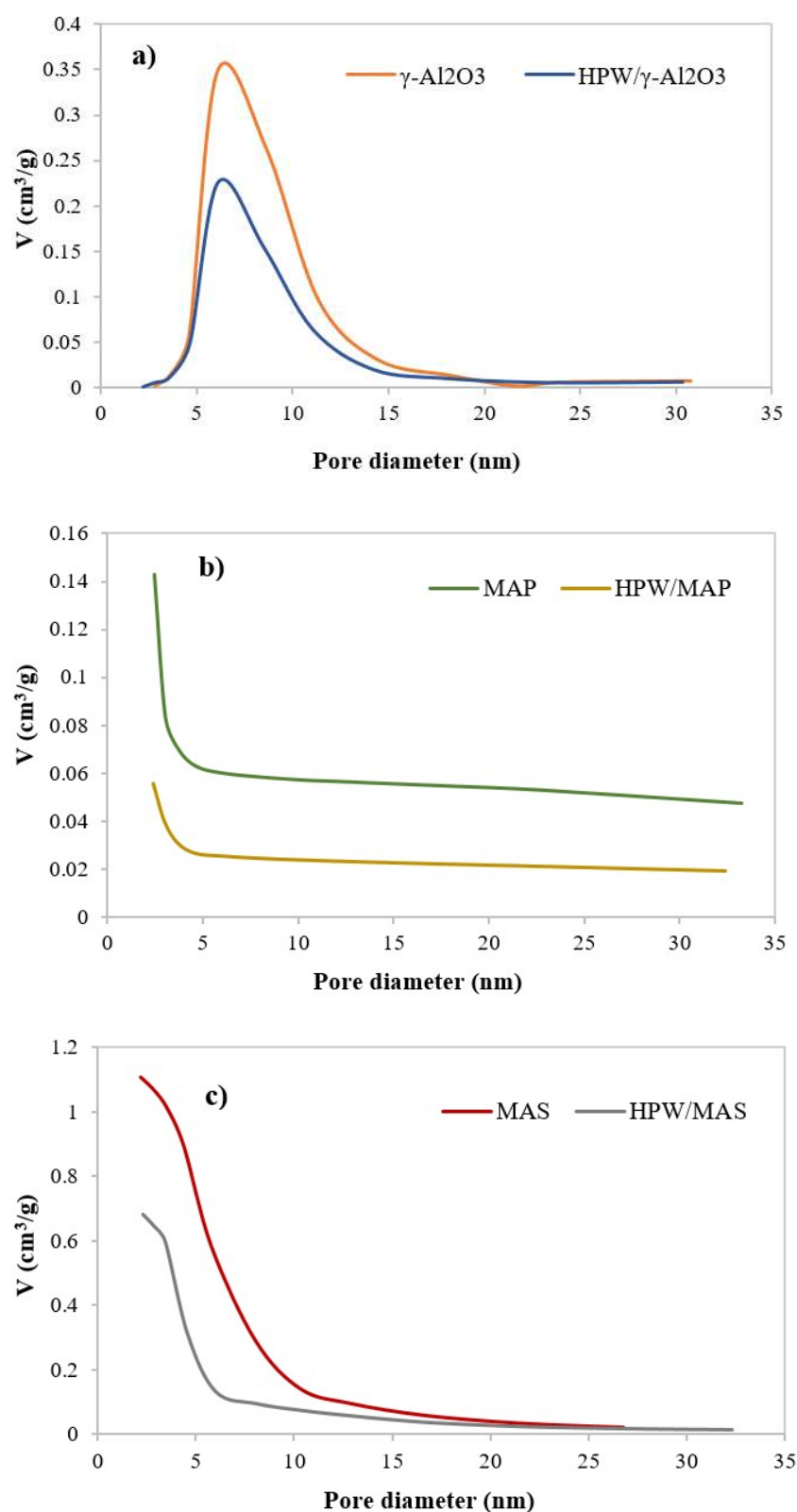


Figure 2. Pore size distribution curves for (a) $\gamma\text{-Al}_2\text{O}_3$ and HPW/ $\gamma\text{-Al}_2\text{O}_3$, (b) MAP and HPW/MAP, and (c) MAS and HPW/MAS.

Pyridine FTIR was carried out to identify the types of acid sites (Bronsted and Lewis acids) in synthesized HPW/MAS, HPW/MAP, and HPW/ $\gamma\text{-Al}_2\text{O}_3$ catalysts. As illustrated in Figure 3, five characteristic peaks at 1446, 1487, 1537, 1600, and 1634 cm^{-1} were observed in all supported HPW catalysts. The band at 1446 cm^{-1} is related to the hydrogen-bonded

pyridine, which correlates to Lewis acid sites. The band at 1487 is attributed to the presence of both Bronsted and Lewis acid sites. The characteristic peaks at around 1537 and 1634 correspond to Bronsted acid sites, while the peak at approximately 1600 can be attributed to the bond formed between pyridine and Al^{3+} Lewis acid sites of all the catalysts. The obtained results confirm the presence of both types of acid sites in the synthesized catalysts [30,33]. Similar procedures were used by Hoo et al. [32] and Sudhakar et al. [34] to determine and discuss catalysts' acidity.

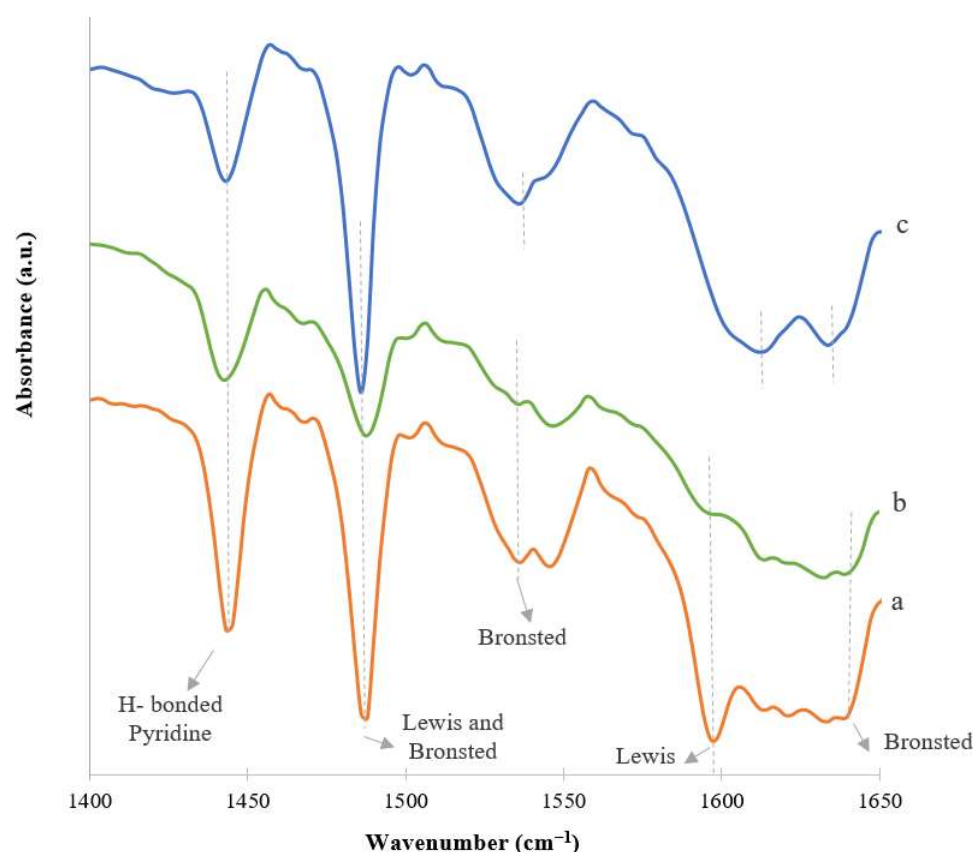


Figure 3. FTIR spectra after pyridine desorption of (a) HPW/MAS, (b) HPW/MAP, and (c) HPW/ γ - Al_2O_3 .

XRD patterns of HPW, γ - Al_2O_3 , HPW/ γ - Al_2O_3 , MAS, HPW/MAS, MAP, and HPW/MAP at a high diffraction angle are exhibited in Figure 4. According to the literature [35], the peaks reflected at $2\theta = 10.3, 20.7, 25.4, 29.5,$ and 34.7° are associated with crystalline HPW structure. Moreover, regarding the crystalline structure of γ - Al_2O_3 , the peaks at $2\theta = 37.1, 46.0,$ and 66.6° are related to the planes of 400 and 440, respectively. However, after immobilization of HPW on the surface of γ - Al_2O_3 , the intensity of the peaks decreased as compared to pure γ - Al_2O_3 , confirming that HPW was well incorporated in the support [36]. Broad peaks in the XRD spectra of MAP, HPW/MAP, MAS, and HPW/MAS in the range of 20 to 30° were noticed, confirming the amorphous structure of the synthesized mesoporous catalysts. The suitable incorporation of Kegging anions on the surface of the support materials verified by XRD, can be attributed to the difference in the pore size of the support materials (γ - $\text{Al}_2\text{O}_3 = 7.5$ nm, MAP = 4.7 nm, and MAS = 5 nm) and the Kegging anions (1.2 nm). This can facilitate the uniform dispersion of HPW on the surface of support materials, preventing agglomeration of HPW.

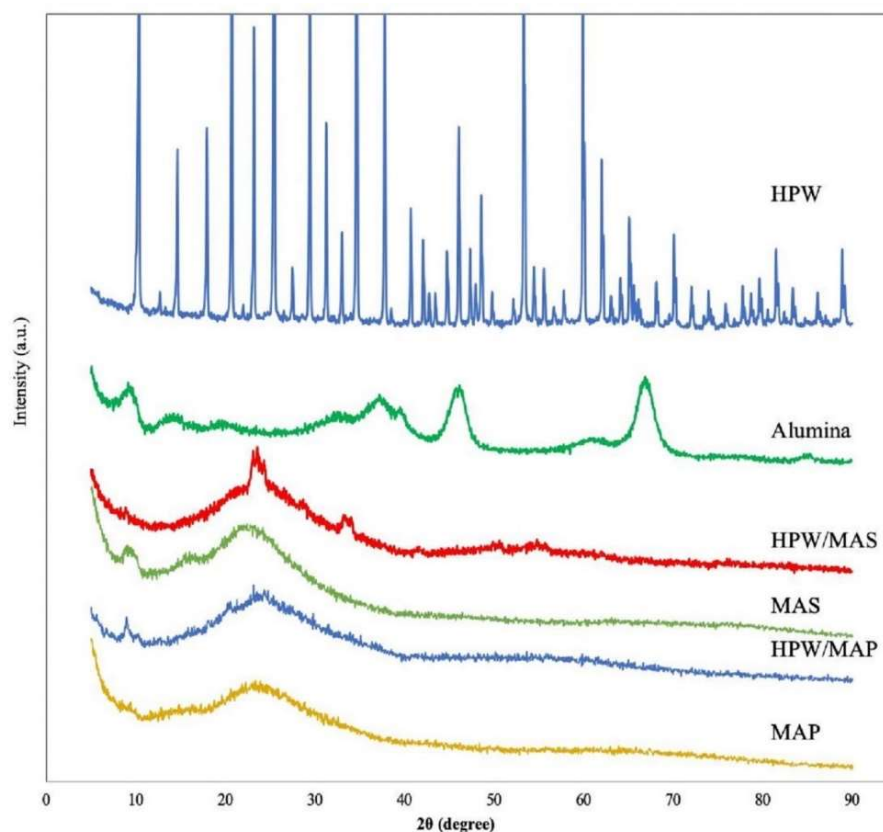


Figure 4. XRD patterns of HPW, γ - Al_2O_3 , and synthesized catalysts.

TEM images of the catalysts are illustrated in Figure 5. The images of HPW/MAS and HPW/MAP show the dispersion of the round particles ascribed to the Keggin anions of HPW distributing on the support materials. The dark circles indicated by arrows in Figure 5b,d, confirm that HPW settled inside the pores of the support materials. The HPW diameter is less than the support material and this difference contributes to residing HPW anions inside the pores. Kurhade et al. [35] and Baddy et al. [37] reported similar observations.

The NH_3 -TPD characterization technique was employed to analyze the acidity of the prepared catalysts. The total acidity and acidity in various temperature intervals for support materials, HPW supported catalysts, and recovered HPW supported catalysts are reported in Table 3. Three temperature intervals of 100–300 °C, 300–500 °C, and 500–600 °C were used for this analysis in Table 3, which can be categorized into mild acidic sites, medium and strong acidic sites, respectively. The acidity strengths of all the HPW supported catalysts were related mainly to the range of 150 to 500 °C, representing medium acidic sites. However, there is presence of weak acidic sites (in the range of 100 to 150 °C) for all the catalysts. The total acidity of the materials was calculated by integrating the curve from the TPD data and comparing the data with those of standard samples in the temperature range from 100 °C to 600 °C.

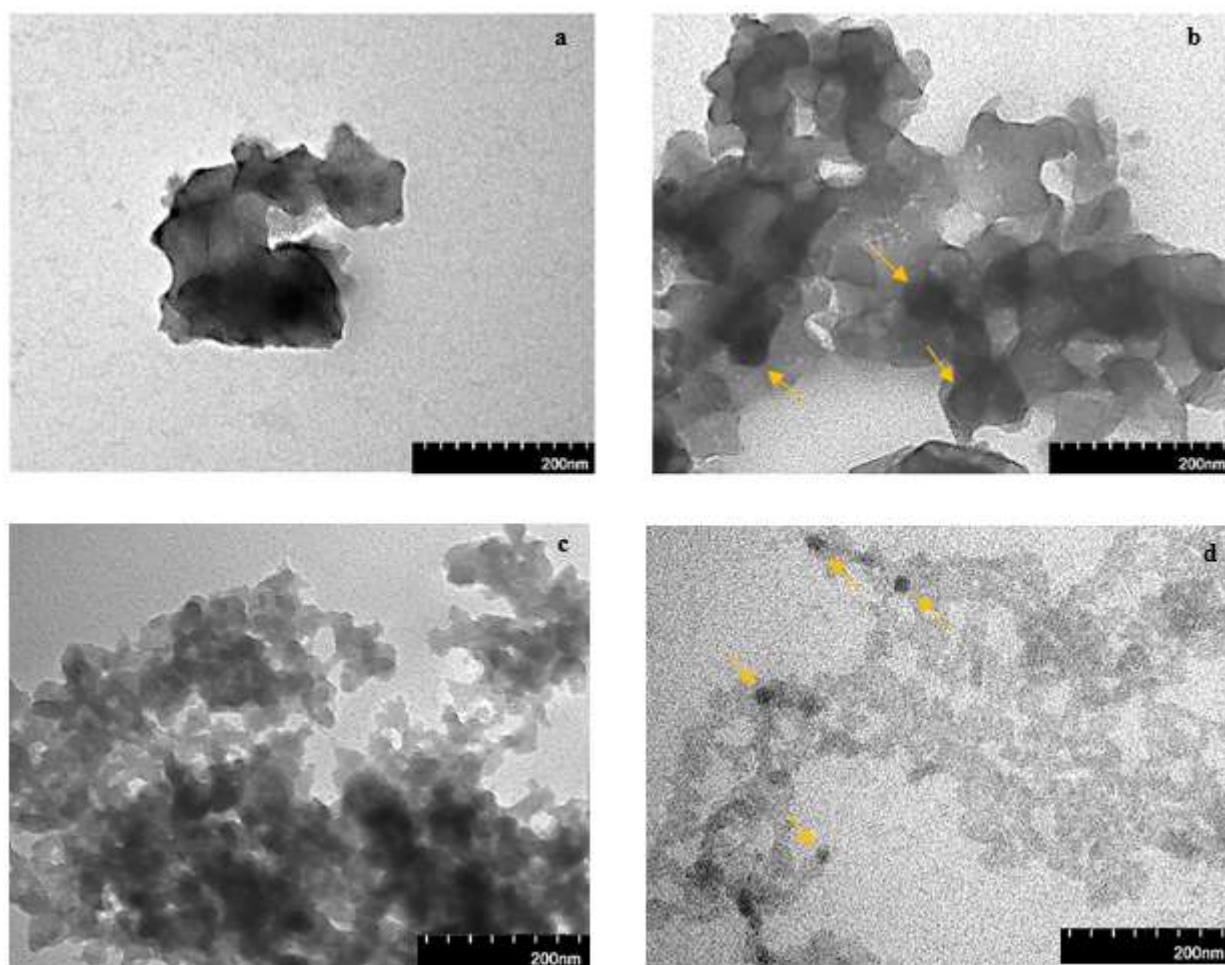


Figure 5. TEM images of (a) MAP, (b) HPW/MAP, (c) MAS, and (d) HPW/MAS.

Table 3. Acidity of support materials and HPW supported catalysts obtained from NH_3 -TPD.

Catalyst	Total Acidity ($\mu\text{mol/g}$)	100–300 °C	300–500 °C	500–600 °C
$\gamma\text{-Al}_2\text{O}_3$	922	354	429	139
HPW/ $\gamma\text{-Al}_2\text{O}_3$	913	328	480	105
R*-HPW/ $\gamma\text{-Al}_2\text{O}_3$	876	332	453	91
MAP	795 \pm 8	283	220	292
HPW/MAP	841	245	348	248
R*-HPW/MAP	835	292	302	241
MAS	1015 \pm 16	270	276	469
HPW/MAS	1111 \pm 13	466	448	196
R*-HPW/MAS	1082	449	565	68

* R—Recovered.

Based on the TPD results (Table 3), the acidity amount of $\gamma\text{-Al}_2\text{O}_3$, MAP, and MAS were obtained of 795 $\mu\text{mol/g}$, 1015, and 922 $\mu\text{mol/g}$, respectively. HPW immobilization on the support materials led to an acidity increase of 9.5% for HPW/MAS and 5.8% for HPW/MAP. Accordingly, HPW/MAS represented higher acidity related to HPW/MAP and HPW/ $\gamma\text{-Al}_2\text{O}_3$. The acidity of HPW supported catalysts was also analyzed after the first recovery from the reaction, which indicated no significant decrease in acidity for HPW/ $\gamma\text{-Al}_2\text{O}_3$ (<5%), HPW/MAP (<1%), and HPW/MAS (<3%) [32,38].

The thermal behavior of the prepared catalysts was examined through thermogravimetric analysis. As represented in Figure 6, the largest weight loss in the TGA profiles of MAP, HPW/MAP, γ -Al₂O₃, and HPW/ γ -Al₂O₃ occurs approximately between 80 °C and 200 °C, while for MAS and HPW/MAS, it is between 50 °C and 150 °C, corresponding to the loss of physically absorbed water molecules. With regard to the support material, more water was physically absorbed by MAP followed by MAS and γ -Al₂O₃, which could be due to the hydrogen bonding established between these support materials and water. Crystallization of Kegging ions also leads to weight loss in HPW supported catalysts, as a result of the loss of water [39]. Thermal stability of the support materials and HPW supported catalysts was determined to be stable up to 600 °C.

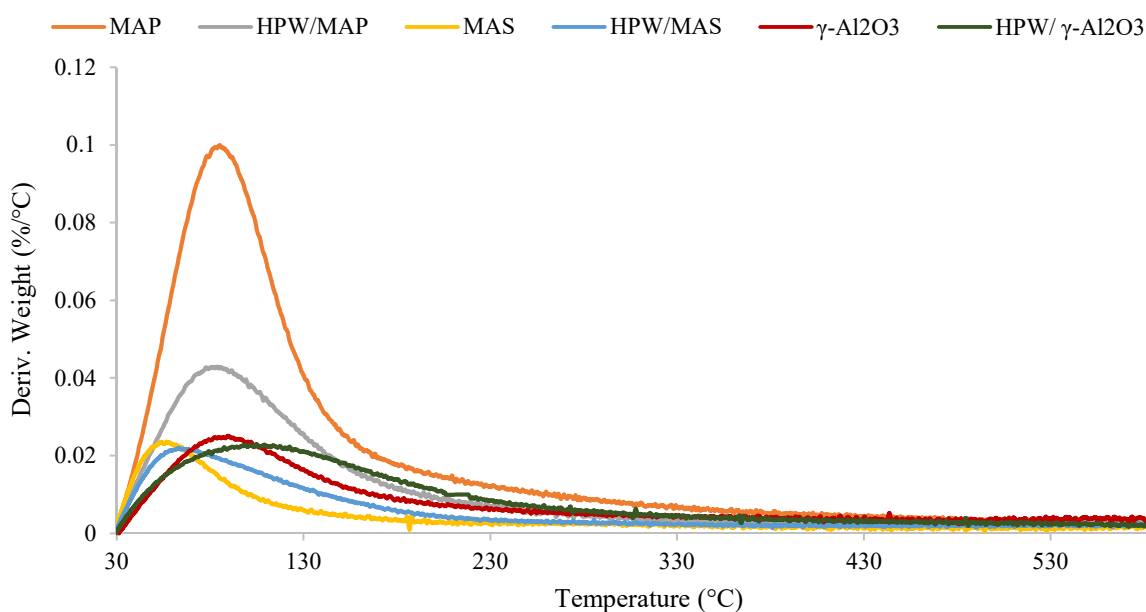


Figure 6. Thermogravimetric analysis of supports (MAP, MAS, and γ -Al₂O₃) and catalysts (HPW/MAP, HPW/MAS, and HPW/ γ -Al₂O₃).

The mechanism of HPW immobilization on MAS is shown in Figure 7. In the first step, the surface hydroxyl groups of synthesized MAS were dehydroxylated by calcination at 500 °C, to create electron donor and acceptor sites. In the second step, HPW was anchored to MAS by the interaction between the H⁺ of the heteropoly anion of HPW and the Al⁺ site of MAS, which creates a negative charge (δ^-) at HPW and leads to the electrostatic attachment of HPW to the Lewis site (Si⁺) of MAS [35,40]. The existence of both Lewis and Bronsted acid sites on the solid acid catalysts is essential in developing simultaneous esterification and transesterification reactions for biodiesel production. A Lewis acid catalyst is favorable to ease the transesterification reaction, while for facilitating the esterification reaction, Bronsted acidic sites play a significant role. Regarding the HPW supported catalysts used in this research study, alumina and the synthesized support materials provide Lewis acid sites, and HPW provides the Bronsted acidic sites. Therefore, immobilization of HPW on these support materials that possess both Bronsted and Lewis acidic sites is favorable for biodiesel production, through simultaneous esterification and transesterification reactions [16,41].

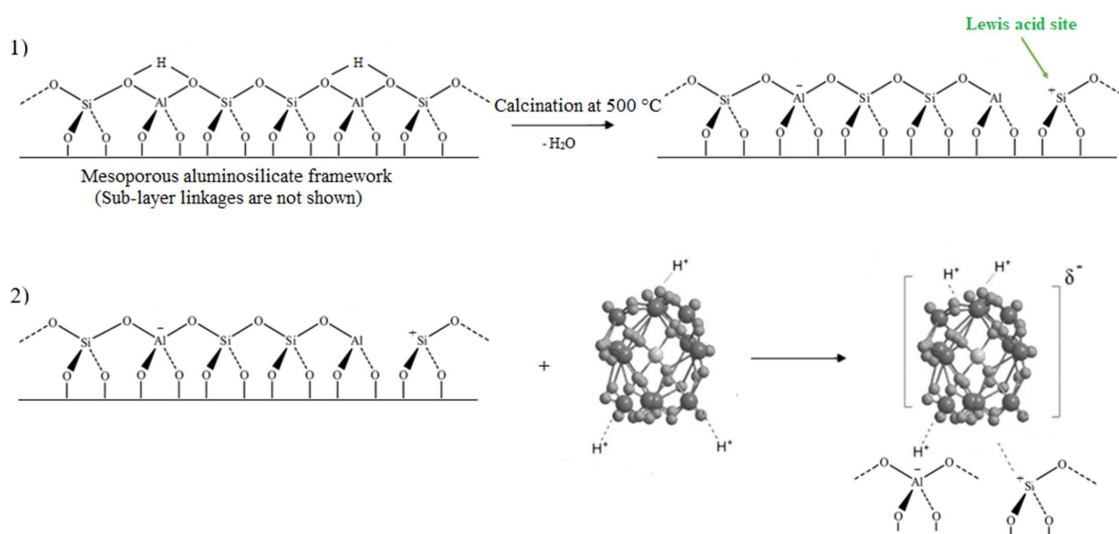


Figure 7. Mechanism of HPW immobilization on MAS including (1) calcination of MAS at 500 °C to obtain Lewis acid sites, and (2) immobilization of HPW with Bronsted acid sites on MAS.

3.2. Catalytic Activity

The performance of the prepared catalysts was screened at a preliminary reaction condition of 3 wt.% catalyst, and a methanol to oil molar ratio of 20:1 at 200 °C and 4 MPa over 7 h. The percentage of biodiesel yield over time at intervals of one hour was reported in Figure 8. According to this figure, the introduction of HPW on the surface of the support materials resulted in a higher biodiesel yield for all of them, as compared to the bare support materials. The methyl ester yield improved for all the catalysts over time; however, the increasing trend was slower in the last 3 h. HPW/MAS indicated a better biodiesel yield of 82.3% in comparison with HPW/MAP and HPW/ γ -Al₂O₃, with 78.3% and 64.2%, respectively. This can be ascribed to the higher surface area and acidity of HPW/MAS confirmed by BET and NH₃-TPD analysis, respectively. Higher surface area enhances the dispersion of the Kegging anions on the surface of HPW, leading to better acidity and higher biodiesel yield. Furthermore, the accomplished results show the superiority of the fabricated catalysts of MAS and MAP, in terms of catalytic activity in simultaneous esterification and transesterification reactions, in comparison with commercial γ -Al₂O₃.

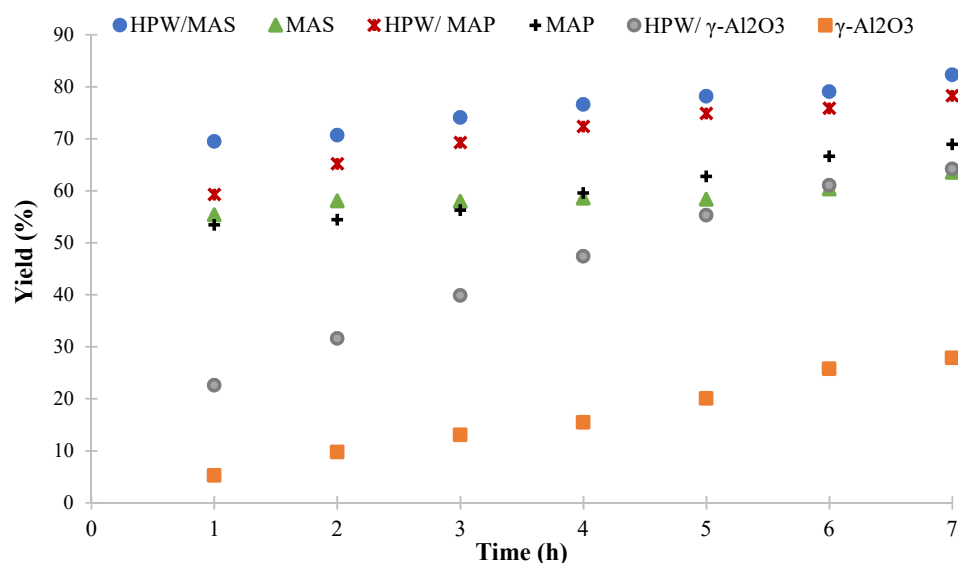


Figure 8. Screening the performance of support materials and HPW supported catalysts for biodiesel production over time (3 wt.% catalyst, methanol to oil molar ratio 20:1, 200 °C, 4 MPa, and 7 h).

Table 4 shows the reaction conditions of some similar work that used HPW supported catalysts for biodiesel production. Accordingly, the amount of catalyst used in this study is less than that in most of the other studies, which can have a significant impact on the cost of production.

Table 4. Tungstophosphoric supported catalysts for biodiesel production.

Catalyst	Reaction Conditions	Conversion or Yield (wt.%)	Ref.
HPA/MK700	Temperature = 200 °C, reaction time = 2 h, alcohol to oil molar ratio = 10, catalyst loading = 10 wt.%	Conversion = 83.0	[29]
H ₄ SiW ₁₂ O ₄₀ -SiO ₂	Temperature = 65 °C, reaction time = 6 h, catalyst loading = 20 wt.%	Yield = 73.0	[28]
TPA/SBA-15	Temperature = 65 °C, reaction time = 8 h, alcohol to oil molar ratio = 8, catalyst loading = 0.3 g	Conversion = 86.0	[42]
TPA/zeolite H β	Temperature = 60 °C, reaction time = 6 h, alcohol to oil molar ratio = 20, catalyst loading = 30 wt.%	Conversion = 84.0	[43]
TPA/SnO ₂	Temperature = 65 °C, reaction time = 200 min, alcohol to oil molar ratio = 14, catalyst loading = 1 g	Conversion = 81.2	[44]
HPW/ γ -Al ₂ O ₃	Temperature = 200 °C, reaction time = 7 h, alcohol to oil molar ratio = 20, catalyst loading = 3 wt.%	Yield = 64.2	This study
HPW/MAP	Temperature = 200 °C, reaction time = 7 h, alcohol to oil molar ratio = 20, catalyst loading = 3 wt.%	Yield = 78.3	This study
HPW/MAS	Temperature = 200 °C, reaction time = 7 h, alcohol to oil molar ratio = 20, catalyst loading = 3 wt.%	Yield = 82.3	This study

The mechanisms of the acid-catalyzed esterification of fatty acid and acid-catalyzed transesterification of triglyceride using HPW supported catalysts are expressed in Figure 9a,b. Accordingly, the interaction of the carbonyl oxygen (C=O) of the fatty acid and triglyceride with the catalyst active site, which is acidic (H⁺), leads to the carbocation. A tetrahedral intermediate is generated after introducing methanol, with a nucleophilic effect on the carbocation. The water in the esterification reaction and glycerol in the transesterification reaction are finally eliminated from the tetrahedral intermediate to form methyl ester and regenerate the catalyst [45,46]. As HPW supported catalysts are not sensitive to water, the formation of water during the reaction has no adverse effect on their catalytic activity, which can be maintained during the process.

3.3. Reusability Study

The main advantage of using heterogeneous catalysts is their reusability, which can reduce the cost of production as catalysts are expensive materials. The reusability of HPW/MAS as the best synthesized catalyst was examined through five cycles, using the same reaction conditions. For this purpose, after each reaction, the catalyst was filtered and regenerated via washing with tetrahydrofuran and hexane to eliminate polar and nonpolar contaminants, followed by drying at 100 °C. According to the reusability results shown in Figure 10, HPW/MAS maintained around 80% of its initial activity after five runs.

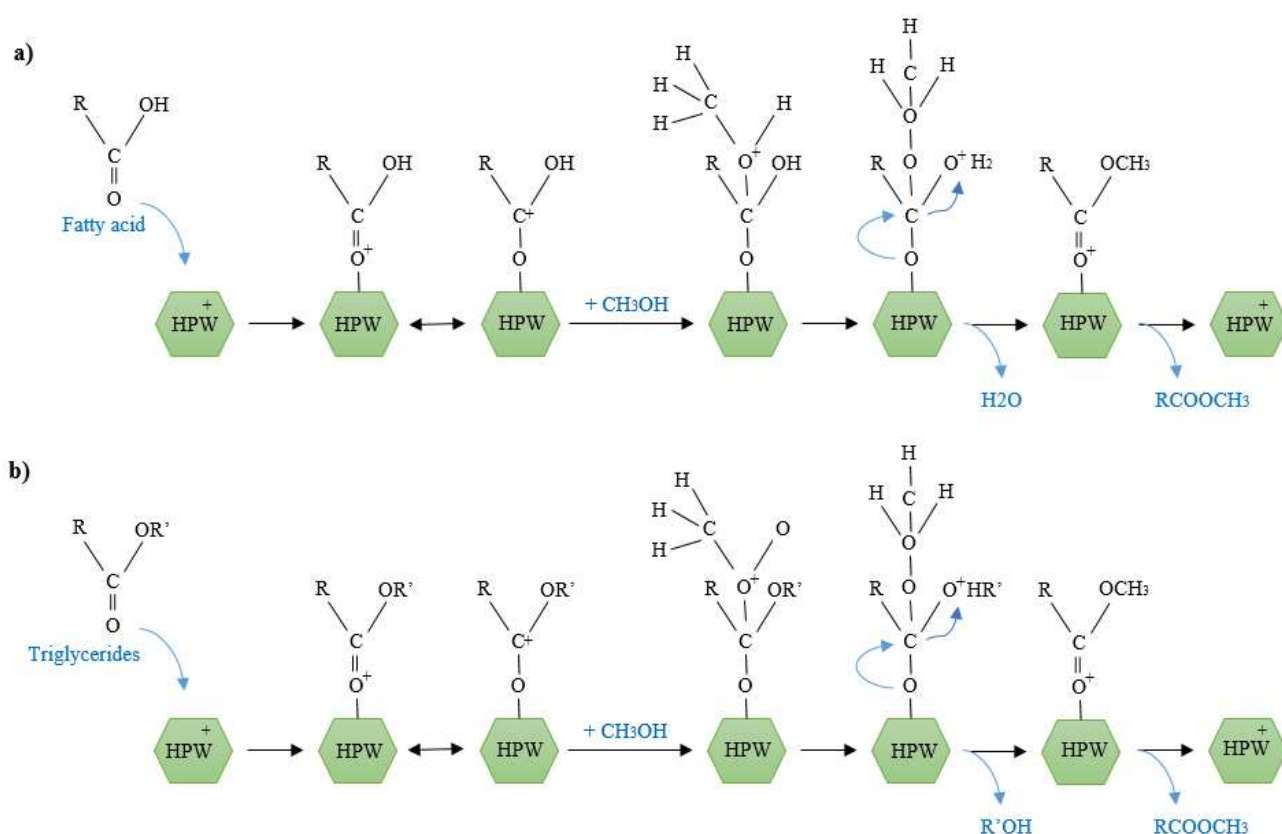


Figure 9. Mechanism of alcoholysis process of (a) esterification reaction and (b) transesterification reaction using HPW anchored to support materials as a solid acid catalyst.

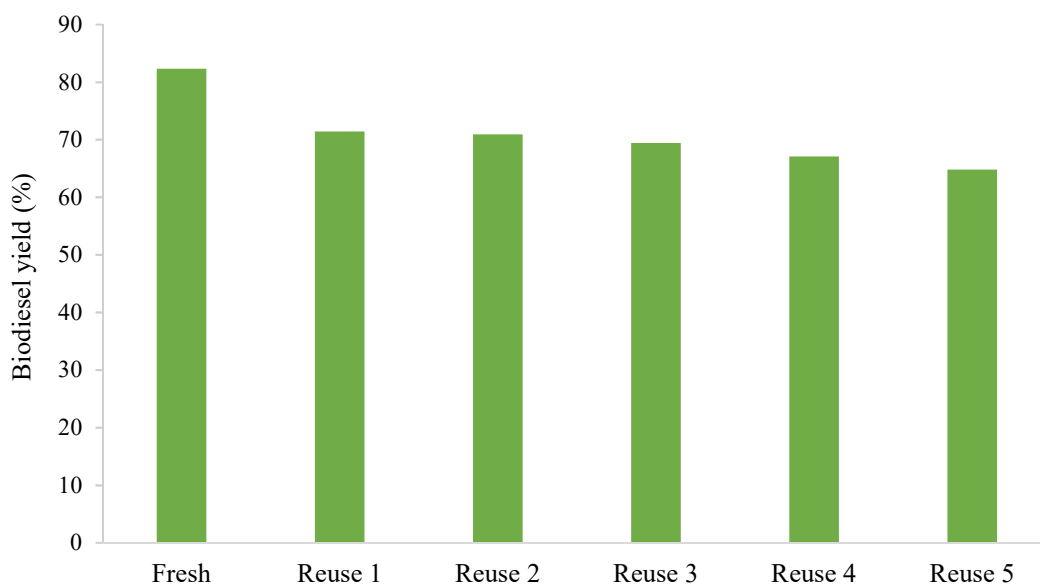


Figure 10. Reusability study of HPW/MAS for biodiesel production over five cycles.

4. Conclusions

The incorporation of HPW on $\gamma\text{-Al}_2\text{O}_3$, MAP, and MAS was studied for simultaneous esterification and transesterification reactions of biodiesel production, using unrefined green seed canola oil. According to the TEM images of HPW/MAP and HPW/MAS, HPW dispersed properly on the surface of the carriers. In addition, the surface area of the catalysts decreases after HPW impregnation, as confirmed by the BET method which

proved the settlement of HPW inside the pores of the support materials. Both synthesized support materials of MAP and MAS provide high surface area and suitable porosity for the immobilization of HPW; however, according to the results obtained, using HPW/MAS led to a better biodiesel yield (82.3%) compared to HPW/MAP (78.3%), which can be attributed to the higher surface area and acidity of HPW/MAS, with 504.3 m²/g and 1111 μmol/g, respectively. A reusability study of HPW/MAS through five cycles indicated high catalytic activity after five successive uses (80% of its initial activity). The results obtained from this study prove that HPW/MAS could be an efficient solid acid catalyst for biodiesel production from feedstocks with low quality, such as unrefined green seed canola oil, which is rich in FFAs, without any pre-treatment processes. However, catalytic activity and reusability could be enhanced by reducing active phase leaching through increasing the interaction between the active phase and support materials. In this regard, the use of suitable linkers such as organosilanes is recommended to be investigated in future studies.

Author Contributions: Conceptualization, F.E. and A.K.D.; methodology, F.E.; formal analysis, F.E.; investigation, F.E. and S.M.; writing—original draft preparation, F.E. and S.M.; writing—review and editing, F.E., S.M. and A.K.D.; visualization, F.E. and S.M.; supervision, A.K.D.; project administration, A.K.D.; funding acquisition, A.K.D. All authors have read and agreed to the published version of the manuscript.

Funding: This research was funded by the Natural Sciences and Engineering Research Council of Canada (NSERC), and the Canada Research Chair (CRC) Program.

Acknowledgments: The authors acknowledge the funding from Natural Sciences and Engineering Research Council of Canada (NSERC) and the Canada Research Chair (CRC) Program.

Conflicts of Interest: The authors declare no conflict of interest.

Abbreviations

ACN	Acetonitrile
BJH	Barrett–Joyner–Halenda
CTAB	Cetyltrimethylammonium bromide
FAAE	Fatty acid alkyl ester
FFAs	Free fatty acids
HPAs	Heteropoly acids
HPW	12-tungstophosphoric heteropoly acid
HPW/MAP	Mesoporous aluminophosphate supported 12-tungstophosphoric heteropoly acid
HPW/MAS	Mesoporous aluminosilicate supported 12-tungstophosphoric heteropoly acid
HPW/γ-Al ₂ O ₃	Gamma alumina supported 12-tungstophosphoric heteropoly acid
MAP	Mesoporous aluminophosphate
MAS	Mesoporous aluminosilicate
NH ₃ -TPD	Temperature-programmed desorption of ammonia
TEOS	Tetraethylorthosilicate
TMAOH	Tetramethyl ammonium hydroxide
TPAOH	Tetrapropyl ammonium hydroxide

References

1. Deshmukh, M.K.G.; Sameeroddin, M.; Abdul, D.; Abdul Sattar, M. Renewable energy in the 21st century: A review. *Mater. Today Proc.* **2021**, *5–8*, In Press. [[CrossRef](#)]
2. Esmi, F.; Nematian, T.; Salehi, Z.; Khodadadi, A.A.; Dalai, A.K. Amine and aldehyde functionalized mesoporous silica on magnetic nanoparticles for enhanced lipase immobilization, biodiesel production, and facile separation. *Fuel* **2021**, *291*, 120126. [[CrossRef](#)]
3. Teimouri, Z.; Abatzoglou, N.; Dalai, A.K. *Kinetics and Selectivity Study of Fischer-Tropsch Synthesis to c5+ Hydrocarbons: A Review*; MDPI: Basel, Switzerland, 2021; Volume 11, ISBN 1306966477.
4. Silvestre, W.P.; Pauletti, G.F.; Baldasso, C. Fodder radish (*Raphanus sativus* L.) seed cake as a feedstock for pyrolysis. *Ind. Crops Prod.* **2020**, *154*, 112689. [[CrossRef](#)]

5. Anish Kumar, K.; Senthil Kumar, P.; Madhusudanan, S.; Pasupathy, V.; Vignesh, P.R.; Sankaranarayanan, A.R. A simplified model for evaluating best biodiesel production method: Fuzzy analytic hierarchy process approach. *Sustain. Mater. Technol.* **2017**, *12*, 18–22. [[CrossRef](#)]
6. Orugba, H.O.; Edomwonyi-Otu, L.C. Improving the activity and stability of turtle shell-derived catalyst in alcoholysis of degraded vegetable oil: An experimental design approach. *J. King Saud Univ. Eng. Sci.* **2021**; *In Press*.
7. Avhad, M.R.; Marchetti, J.M. A review on recent advancement in catalytic materials for biodiesel production. *Renew. Sustain. Energy Rev.* **2015**, *50*, 696–718. [[CrossRef](#)]
8. Chozhavendhan, S.; Vijay Pradhap Singh, M.; Fransila, B.; Praveen Kumar, R.; Karthiga Devi, G. A review on influencing parameters of biodiesel production and purification processes. *Curr. Res. Green Sustain. Chem.* **2020**, *1–2*, 1–6. [[CrossRef](#)]
9. Wong, K.Y.; Ng, J.H.; Chong, C.T.; Lam, S.S.; Chong, W.T. Biodiesel process intensification through catalytic enhancement and emerging reactor designs: A critical review. *Renew. Sustain. Energy Rev.* **2019**, *116*, 109399. [[CrossRef](#)]
10. Pritchard, J.; Filonenko, G.A.; Van Putten, R.; Hensen, E.J.M.; Pidko, E.A. Heterogeneous and homogeneous catalysis for the hydrogenation of carboxylic acid derivatives: History, advances and future directions. *Chem. Soc. Rev.* **2015**, *44*, 3808–3833. [[CrossRef](#)]
11. Astruc, D. Introduction: Nanoparticles in Catalysis. *Chem. Rev.* **2020**, *120*, 461–463. [[CrossRef](#)]
12. Xiao, T.; Yabushita, M.; Nishitoba, T.; Osuga, R.; Yoshida, M.; Matsubara, M.; Maki, S.; Kanie, K.; Yokoi, T.; Cao, W.; et al. Organic Structure-Directing Agent-Free Synthesis of Mordenite-Type Zeolites Driven by Al-Rich Amorphous Aluminosilicates. *ACS Omega* **2021**, *6*, 5176–5182. [[CrossRef](#)]
13. Rattanaphra, D.; Harvey, A.P.; Thanapimmetha, A.; Srinophakun, P. Kinetic of myristic acid esterification with methanol in the presence of triglycerides over sulfated zirconia. *Renew. Energy* **2011**, *36*, 2679–2686. [[CrossRef](#)]
14. Niu, M.; Kong, X. Efficient biodiesel production from waste cooking oil using p-toluenesulfonic acid doped polyaniline as a catalyst. *RSC Adv.* **2015**, *5*, 27273–27277. [[CrossRef](#)]
15. Surasit, C.; Yoosuk, B.; Pohmakotr, M.; Tantirungrotechai, J. Biodiesel Synthesis from Palm Fatty Acid Distillate Using Tungstophosphoric Acid Supported on Cesium-Containing Niobia. *JAOS J. Am. Oil Chem. Soc.* **2017**, *94*, 465–474. [[CrossRef](#)]
16. Gaurav, A.; Dumas, S.; Mai, C.T.Q.; Ng, F.T.T. A kinetic model for a single step biodiesel production from a high free fatty acid (FFA) biodiesel feedstock over a solid heteropolyacid catalyst. *Green Energy Environ.* **2019**, *4*, 328–341. [[CrossRef](#)]
17. Negm, N.A.; Sayed, G.H.; Yehia, F.Z.; Habib, O.I.; Mohamed, E.A. Biodiesel production from one-step heterogeneous catalyzed process of Castor oil and Jatropha oil using novel sulphonated phenyl silane montmorillonite catalyst. *J. Mol. Liq.* **2017**, *234*, 157–163. [[CrossRef](#)]
18. Alipour, Z.; Rezaei, M.; Meshkani, F. Effects of support modifiers on the catalytic performance of Ni/Al₂O₃ catalyst in CO₂ reforming of methane. *Fuel* **2014**, *129*, 197–203. [[CrossRef](#)]
19. Mansir, N.; Taufiq-Yap, Y.H.; Rashid, U.; Lokman, I.M. Investigation of heterogeneous solid acid catalyst performance on low grade feedstocks for biodiesel production: A review. *Energy Convers. Manag.* **2017**, *141*, 171–182. [[CrossRef](#)]
20. Parangi, T.; Mishra, M.K. Solid Acid Catalysts for Biodiesel Production. *Comments Inorg. Chem.* **2020**, *40*, 176–216. [[CrossRef](#)]
21. Gromov, N.V.; Medvedeva, T.B.; Sorokina, K.N.; Samoylova, Y.V.; Rodikova, Y.A.; Parmon, V.N. Direct Conversion of Microalgae Biomass to Formic Acid under an Air Atmosphere with Soluble and Solid Mo-V-P Heteropoly Acid Catalysts. *ACS Sustain. Chem. Eng.* **2020**, *8*, 18947–18956. [[CrossRef](#)]
22. Baroi, C.; Dalai, A.K. Review on biodiesel production from various feedstocks using 12-tungstophosphoric acid (TPA) as a solid acid catalyst precursor. *Ind. Eng. Chem. Res.* **2014**, *53*, 18611–18624. [[CrossRef](#)]
23. Esmi, F.; Borugadda, V.B.; Dalai, A.K. Heteropoly acids as supported solid acid catalysts for sustainable biodiesel production using vegetable oils: A Review. *Catal. Today*, **2022**; *In Press*.
24. Su, F.; Guo, Y. Advancements in solid acid catalysts for biodiesel production. *Green Chem.* **2014**, *16*, 2934–2957. [[CrossRef](#)]
25. Gong, S.W.; Lu, J.; Wang, H.H.; Liu, L.J.; Zhang, Q. Biodiesel production via esterification of oleic acid catalyzed by picolinic acid modified 12-tungstophosphoric acid. *Appl. Energy* **2014**, *134*, 283–289. [[CrossRef](#)]
26. Srilatha, K.; Lingaiah, N.; Sai Prasad, P.S.; Prabhavathi Devi, B.L.A.; Prasad, R.B.N. Kinetics of the esterification of palmitic acid with methanol catalyzed by 12-tungstophosphoric acid supported on ZrO₂. *React. Kinet. Mech. Catal.* **2011**, *104*, 211–226. [[CrossRef](#)]
27. Kumbar, S.M.; Shanbhag, G.V.; Lefebvre, F.; Halligudi, S.B. Heteropoly acid supported on titania as solid acid catalyst in alkylation of p-cresol with tert-butanol. *J. Mol. Catal. A Chem.* **2006**, *256*, 324–334. [[CrossRef](#)]
28. Yan, K.; Wu, G.; Wen, J.; Chen, A. One-step synthesis of mesoporous H₄SiW₁₂O₄₀-SiO₂ catalysts for the production of methyl and ethyl levulinate biodiesel. *Catal. Commun.* **2013**, *34*, 58–63. [[CrossRef](#)]
29. Pires, L.H.O.; de Oliveira, A.N.; Monteiro, O.V., Jr.; Angélica, R.S.; da Costa, C.E.F.; Zamian, J.R.; do Nascimento, L.A.S.; Filho, G.N.R. Esterification of a waste produced from the palm oil industry over 12-tungstophosphoric acid supported on kaolin waste and mesoporous materials. *Appl. Catal. B Environ.* **2014**, *160–161*, 122–128. [[CrossRef](#)]
30. Kurhade, A.; Zhu, J.; Hu, Y.; Dalai, A.K. Surface Investigation of Tungstophosphoric Acid Supported on Ordered Mesoporous Aluminosilicates for Biodiesel Synthesis. *ACS Omega* **2018**, *3*, 14064–14075. [[CrossRef](#)] [[PubMed](#)]
31. Roschat, W.; Siritanon, T.; Yoosuk, B.; Sudyoasuk, T.; Promarak, V. Rubber seed oil as potential non-edible feedstock for biodiesel production using heterogeneous catalyst in Thailand. *Renew. Energy* **2017**, *101*, 937–944. [[CrossRef](#)]

32. Hoo, P.Y.; Abdullah, A.Z. Direct synthesis of mesoporous 12-tungstophosphoric acid SBA-15 catalyst for selective esterification of glycerol and lauric acid to monolaurate. *Chem. Eng. J.* **2014**, *250*, 274–287. [[CrossRef](#)]
33. Kurhade, A.; Zhu, J.; Dalai, A.K.; Zhu, J.; Hu, Y.; Dalai, A.K. Meso-Structured HPW-MAS-7 and HPW-MAS-9 Composite Catalysts for Biodiesel Synthesis from Unrefined Green Seed Canola Oil. *Fuel Process. Technol.* **2018**, *3*, 14064–14075.
34. Sudhakar, P.; Pandurangan, A. Heteropolyacid (H₃PW₁₂O₄₀)-impregnated mesoporous KIT-6 catalyst for green synthesis of bio-diesel using transesterification of non-edible neem oil. *Mater. Renew. Sustain. Energy* **2019**, *8*, 22. [[CrossRef](#)]
35. Kurhade, A.; Dalai, A.K. Physicochemical characterization and support interaction of alumina-supported heteropolyacid catalyst for biodiesel production. *Asia-Pacific J. Chem. Eng.* **2018**, *13*, e2249. [[CrossRef](#)]
36. Tayebbe, R.; Amini, M.M.; Akbari, M.; Aliakbari, A. A novel inorganic-organic nanohybrid material H₄SiW₁₂O₄₀/pyridino-MCM-41 as efficient catalyst for the preparation of 1-amidoalkyl-2-naphthols under solvent-free conditions. *Dalt. Trans.* **2015**, *44*, 9596–9609. [[CrossRef](#)] [[PubMed](#)]
37. Badday, A.S.; Abdullah, A.Z.; Lee, K.T. Ultrasound-assisted transesterification of crude Jatropha oil using alumina-supported heteropolyacid catalyst. *Appl. Energy* **2013**, *105*, 380–388. [[CrossRef](#)]
38. Sawant, D.P.; Vinu, A.; Jacob, N.E.; Lefebvre, F.; Halligudi, S.B. Formation of nanosized zirconia-supported 12-tungstophosphoric acid in mesoporous silica SBA-15: A stable and versatile solid acid catalyst for benzylation of phenol. *J. Catal.* **2005**, *235*, 341–352. [[CrossRef](#)]
39. Brahmkhatri, V.; Patel, A. 12-Tungstophosphoric acid anchored to SBA-15: An efficient, environmentally benign reusable catalysts for biodiesel production by esterification of free fatty acids. *Appl. Catal. A Gen.* **2011**, *403*, 161–172. [[CrossRef](#)]
40. Madhusudhan Rao, P.; Wolfson, A.; Kababya, S.; Vega, S.; Landau, M.V. Immobilization of molecular H₃PW₁₂O₄₀ heteropolyacid catalyst in alumina-grafted silica-gel and mesostructured SBA-15 silica matrices. *J. Catal.* **2005**, *232*, 210–225. [[CrossRef](#)]
41. Gupta, J.; Agarwal, M.; Dalai, A.K. An overview on the recent advancements of sustainable heterogeneous catalysts and prominent continuous reactor for biodiesel production. *J. Ind. Eng. Chem.* **2020**, *88*, 58–77. [[CrossRef](#)]
42. Narkhede, N.; Brahmkhatri, V.; Patel, A. Efficient synthesis of biodiesel from waste cooking oil using solid acid catalyst comprising 12-tungstosilicic acid and SBA-15. *Fuel* **2014**, *135*, 253–261. [[CrossRef](#)]
43. Patel, A.; Narkhede, N. 12-tungstophosphoric acid anchored to zeolite H β : Synthesis, characterization, and biodiesel production by esterification of oleic acid with methanol. *Energy and Fuels* **2012**, *26*, 6025–6032. [[CrossRef](#)]
44. Srilatha, K.; Ramesh Kumar, C.; Prabhavathi Devi, B.L.A.; Prasad, R.B.N.; Sai Prasad, P.S.; Lingaiah, N. Efficient solid acid catalysts for esterification of free fatty acids with methanol for the production of biodiesel. *Catal. Sci. Technol.* **2011**, *1*, 662–668. [[CrossRef](#)]
45. Fan, M.; Si, Z.; Sun, W.; Zhang, P. Sulfonated ZrO₂-TiO₂ nanorods as efficient solid acid catalysts for heterogeneous esterification of palmitic acid. *Fuel* **2019**, *252*, 254–261. [[CrossRef](#)]
46. Hanif, M.A.; Nisar, S.; Rashid, U. Supported solid and heteropoly acid catalysts for production of biodiesel. *Catal. Rev. Sci. Eng.* **2017**, *59*, 165–188. [[CrossRef](#)]